Development of generalized loss functions for rapid estimation of flood damages: a case study in Kelani River basin, Sri Lanka

Akinola Adesuji Komolafe, Srikantha Herath & Ram Avtar

Applied Geomatics

ISSN 1866-9298

Appl Geomat
DOI 10.1007/s12518-017-0200-4

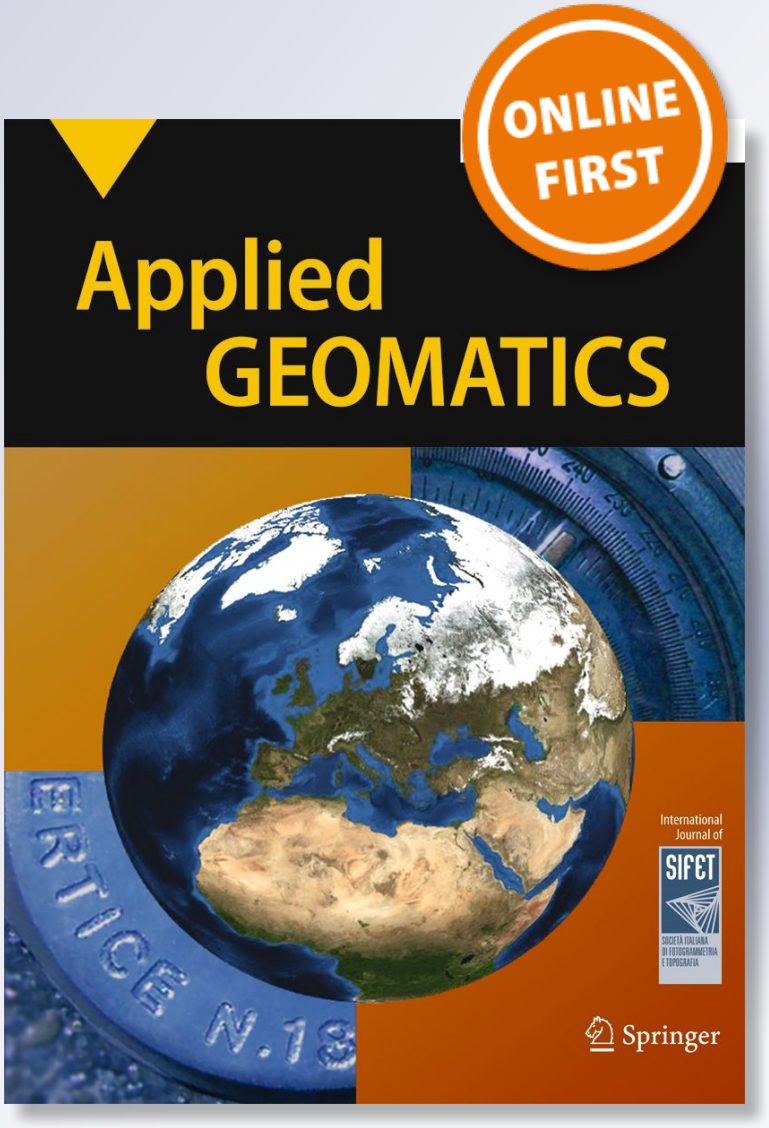

Springer

Applied Geomatics
https://doi.org/10.1007/s12518-017-0200-4

ORIGINAL PAPER

Development of generalized loss functions for rapid estimation of flood damages: a case study in Kelani River basin, Sri Lanka

Akinola Adesuji Komolafe [1,2] · Srikantha Herath [1,3] · Ram Avtar [1,4]

Received: 9 September 2017 / Accepted: 10 November 2017

Abstract Assessment of infrastructural vulnerability to natural hazards, and subsequent economic loss, can make important contributions to future disaster risk minimization. The recent endeavor is to ascertain and evaluate risk globally, which can provide a framework to identify unique regional vulnerabilities, the mobilization of international investments, and cross-country risk comparison. This would require a concerted effort for the detailed classification of building exposures and vulnerability models. This study presents the design and efficacy of flood-vulnerability models for structural building types. The study uses an empirical approach, with data gathered from survey questionnaire, for direct estimation of flood damages in the Kelani River basin in Sri Lanka. Survey questionnaires were administered in the flood-prone areas of the basin, and depth-damage functions were established for four (4) structural building types that were identified based on the relationship between inundation depths and flood damage ratio. Event-based flood hazards were simulated using the Flo-2D model. Building exposures and densities were derived from remote sensing data, using integrated thematic land cover feature indices and supervised image classification. A modified mathematical loss model was employed to simulate flood damages to each building category for a disastrous flood event in the Kelani River basin. Simulated damages and post-flood survey showed reasonable comparativeness. The models can be employed for loss estimation of future damages and risk-reduction planning for flood disaster in Sri Lanka.

Keywords Loss functions · Exposure · Global risk assessment · Disaster risk reduction · Flood damage estimation · GIS · Flood hazards

Introduction

Flood-prone areas of the world are burdened with many risks resulting from increasing exposures and economic activities, and with climate change, there will be greater exposure to extreme weather events and an increase in flood impact (Giang et al. 2009). Preparedness for these events requires adequate estimation of potential risks for effective adaptation measures and mitigation. Traditionally, flood-risk analyses examine the characteristics of flood hazards and the gravity of different events, which are displayed on maps denoting potential risk. To enhance understanding of flood extent and depth analysis, various hydrological models have been developed to ensure accuracy and reduce large uncertainties of flood simulation outputs (Cammerer et al. 2013; Freni et al. 2010; Merz et al. 2010; Moel and Aerts 2011). Notwithstanding, potential consequences of flood hazards are not well determined, regarding specific vulnerabilities, which are often expressed in monetary terms (Cammerer et al. 2013). For this reason, many approaches have been developed to evaluate flood economic damages (Dutta and Herath 2001; Dutta et al. 2003; Herath et al. 1999).

Typical post-flood surveys are laborious and time consuming, giving rise to the flood damage modeling approach (Giang et al. 2009; Islam and Ado 2000; Merz et al. 2010). In recent years, flood damage modeling has witnessed growing attention as a prominent component of flood-risk analysis (Dutta and Herath 2001; Dutta et al. 2003; Heisten and Davdge 2005; Herath et al. 1999; Islam and Ado 2000; Merz et al. 2010). Although it is relatively new (Cammerer et al. 2013), it has become vital, given that most flood-risk

✉ Akinola Adesuji Komolafe
aakomolafe@futa.edu.ng

[1] Institute for the Advanced Study of Sustainability, United Nations University, 5 Chome-53-70 Jingumae, Shibuya, Tokyo 150-8925, Japan

[2] Department of Remote Sensing and Geoscience Information System (GIS), Federal University of Technology, P.M.B. 704, Akure, Ondo State, Nigeria

[3] Ministry of Megapolis and Western Development, Battaramulla 10120, Sri Lanka

[4] Graduate School of Environmental Science, Hokkaido University, Sapporo, Japan

Published online: 30 November 2017

reduction investments are based on cost benefits analysis (CBA). Calculation of flood economic damage is performed by scientific communities and policy makers for flood-risk prevention and reduction, assessment of flood vulnerability, flood-risk mapping, deliberation on flood mitigation measures, comparative risk analysis, and financial appraisals for re-insurance sector and financial appraisals during and immediate after floods (Cammerer and Thieken 2013; Cammerer et al. 2013; Dutta et al. 2003; Herath et al. 1999; James and Hall 1986; Merz et al. 2010). Rapid estimation of flood damages utilizes stage-damage curves from which mathematical functions are generated and integrated with flood hazard characteristics, exposures, and the value of elements at risk (Dutta et al. 2003; Herath et al. 1999; Herath and Wang 2009). These are then simulated using geographical information systems (GIS) to estimate both aftermath and potential damages of various flood scenarios. Stage-damage functions (known as vulnerability or loss functions) are an integral component of risk analysis, particularly for estimating economic losses from flood disasters. It establishes relationship between the rate of flood damage categories and flood characteristics, such as water depths, duration, velocity, and sediments. Several studies have been done considering flood water depths as the primary source of damages. Other flood characteristics, such as wind, velocity, and duration, have also been investigated (Herath and Wang 2009; Kelman and Spence 2004; Kreibich et al. 2005). Accuracy of the damage estimation has been investigated by different scholars (Freni et al. 2010; Jonkman et al. 2008; Komolafe et al. 2015; Notaro et al. 2014). Sources of these uncertainties have largely been attributed to the complex nature of flood-wave propagation processes (especially in urban watersheds), lack of data for validation and calibration, insufficient damage modeling approaches, landuse data, and incomplete flood damage classification.

Flood damage classification is a major contribution to damage estimation. Flood damage categories are classified as tangible and intangible. Tangibles are further classified as direct and indirect. Direct damages are caused by concrete contact with flood water, such as loss of life. Indirect damages are abstract impacts, such as emotional trauma or loss of productivity and income (Jongman et al. 2012). Damage and loss estimations have been derived for various categories of tangible properties, such as residential, commercial, and agricultural crops (Dutta and Herath 2001; Dutta et al. 2003; Herath et al. 1999; Kreibich et al. 2005). Most of these categories are aggregated and do not reflect detailed components of different structural responses to flood water. More detailed unified loss functions, that are applicable globally, are required to enable the comparison of losses between countries, which would lend access to common adaptation and mitigation sources. Also, subdividing building exposures to ultra-specific categories, according to de Moel et al. (2012), would allow for more detailed stage-damage functions and improved differentiation of economic values at risk. The objective of this study is to present and validate vulnerability functions for global building types in the Kelani River basin, Colombo, for urban river flood disaster risk management, as classified by the United Nations office of Disaster Risk Reduction (UNISDR) in Kelani basin, Colombo, Sri Lanka.

A number of studies have been carried out on flood damage assessment in Sri Lanka, despite incessant occurrences of floods caused by excessive rains. Most of these studies are based on post-flood surveys by the Ministry of Disaster Management and World Bank (DMC 2010). Other scholars have attempted to develop loss functions for the estimation of flood damages in Sri Lanka concentrating primarily on the impact of the 2004 Indian Ocean Tsunami flood (Kimura et al. 2006; Murao and Nakazato 2010; Peris 2006). Sri Lanka was one of the most affected countries by the Indian Ocean Tsunami in 2004, with about 40,000 human casualties and 96,000 homes destroyed (Murao and Nakazato 2010). A tsunami is a series of long massive waves generated by an undersea disturbance caused by earthquake or volcanic eruption under the Ocean. These immense waves devastate most coastal dwelling places due to gross elevated flood rising. Stage-damage curves, in response to tsunami floods, were generated from field surveys (Kimura et al. 2006; Murao and Nakazato 2010) and data captured by the Department of Census and Statistics of Sri Lanka (Peris 2006). Fragility curves were constructed taking into account the relationships between building damages and tsunami heights of major coastal cities in Sri Lanka. Implementing established functions, such as fragility curves, has good merit for urban safety planning for catastrophic or natural disasters. However, such functions may not be applicable when preparing for damages caused by urban flooding, arising from excessive rainfalls or river overflow. Urban river flooding from gross rainfall is a recurring event in Sri Lanka and should be afforded priority in future disaster risk-reduction planning. Sri Lanka often experiences flooding and other climatic-related disasters. Flood events, which occur almost every year during monsoon seasons (April to June and September to November), are threats to most of the river basins in the country, especially the study area (Kelani), Kalu, and Gin River basins (Niroshinie et al. 2011).

The study area

The Kelani River basin is one of the most vulnerable basins in Sri Lanka. It stretches to approximately 192 km long with a catchment area of about 2,292km^2. It is the fourth longest river in Sri Lanka. The river flow, which mostly depends on the season, and the three operational reservoirs, is an average of 25m^3/s in dry periods and ranges between 800 and 1500 m^3/s during rainy seasons (Ministry of Irrigation Resources, S. L. 2009). The catchment is naturally divided into two: the steep

and flat terrain (based on the topography), comprised of the upper and the lower catchment, respectively (Fig. 1). The lower catchment is a plain area that receives much water from the upper basin, which often results in overflow. Compounded with poor drainage systems, there is continuous flooding in this area. The average annual rainfall is estimated to be about 3450 mm and a total rainfall of about 6000 mm yearly. The lower part of the basin (about 500km^2) lies within most parts of the Colombo District, which is the most densely populated area and is the hub of commercial activities of Sri Lanka. Because of the high flood risk it poses to Colombo, the commercial capital city (largest city in the country), a comprehensive flood-risk evaluation, encompassing flood forecasting to flood-risk modeling, is very essential to assuage or circumvent disaster risk in this region, as well as the entire country. Historically, most devastating flood events, which resulted in ruin to both public and private properties, were recorded in years 1989, 1992, 2005, 2008, and 2010 (DMC 2010; Niroshine 2012). The basin is projected to experience a series of disastrous flood events as a consequence of climate change, which will inevitably result in tremendous losses, especially in Colombo City. Estimating potential damages that could occur from various weather events is greatly essential to effectively plan for disaster risk reduction and risk management. This can be achieved by utilizing loss functions for efficient estimation of expected damages.

Methodology

To meet this study's objective—to establish and validate loss functions for global building types—event-based inundation extents and depths were simulated using hydrodynamic models to enable detailed survey in the flood-affected areas within the basin. Stage-damage function curves were developed from the acquired empirical damage data. The exposures were mapped with the aid of remote sensing data. The flood hazards, stage-damage functions, exposures, and values of element at risk were integrated in GIS to estimate the flood damages for each building structure for the simulated historical flood event. The results of the total damages were compared with the observed damage data to validate the loss models.

Flood inundation modeling

An event-based approach was applied for comparison and validation of the output from the flood model and economic risks. Data can be readily gleaned from flood hazards, on the extent and intensity. Identification and mapping of flood hazards, for a specific event, are important aspects of flood-risk assessment. Although multiple flood characteristics (e.g., water depths, duration, sediment, wind, and velocity) are responsible for damages in any flood event, water depth is considered in this study as a major damage factor to urban building structures. Flood simulation was performed (for May 2010 flood events in Kelani River basin) using SHER model (Herath et al. 1992; Herath et al. 1990) within the NK_GIAS GIS framework and Flo-2D model. The basin was divided into two: lower Kelani (downstream) and upper Kelani (upstream). The upstream, with high elevation, receives much rainwater and subsequently discharges into the downstream (made mostly of residential and commercial areas), which often resulted into floods. The flow that discharges from upstream was simulated using the SHER model. The inundation modeling was done using Flo-2D with the outflow of the upstream, as the inflow to the downstream. Flo-2D is an integrated GIS and hydrological model (by Flo-2D Software, INC, Arizona, USA). It is a volume conservation flood-routing model that can be used to simulate overland and channel flow over a complex topography. It is also a physical process model that routes rainfall-runoff and flood hydrographs over unconfined flow surfaces or in channels using the dynamic wave approximation to the momentum equation (Flo-2D 2009). Its two-dimensional flood-routing capabilities are accomplished by numerically integrating the equation of motion and conservation of volume for flood water. The distribution of flood waves within the flow domain is controlled by topography and resistance to flow (Flo-2D 2009). The software is a grid-based system that makes use of the interface, Grid Developer System (GDS), with the ability to simulate floods, using various grid attributes, such as rainfall and infiltration, hydraulic structures, channels, levees, n values, and evaporation (Flo-2D 2009).

Governing equations

The Flo-2D model is made up of general fluid equations: the continuity and dynamic wave momentum (motion equation), as displayed in Eqs. 1 and 2.

$$\frac{\partial h}{\partial t} + \frac{\partial hV}{\partial x} = i \tag{1}$$

$$S_f = S_o - \frac{\partial h}{\partial x} - \frac{V}{g}\frac{\partial V}{\partial x} - \frac{1}{g}\frac{\partial V}{\partial t} \tag{2}$$

where h is the flow depth and V is the depth-average velocity in one of the eight flow directions x. I, S_f, and S_o denote the excessive rainfall intensity and friction slope, which is determined by the manning equation and the bed slope pressure gradient, respectively. The equation actually represents one-dimensional depth-average flow; however, because the Flo-2D is a multi-directional flow model (eight potential flow directions), the equations are applied over grid elements, by computing average velocity flow in one direction at a time (Flo-2D 2009). The eight flow directions are the following: the four cardinal directions (north, south, east, and west) and

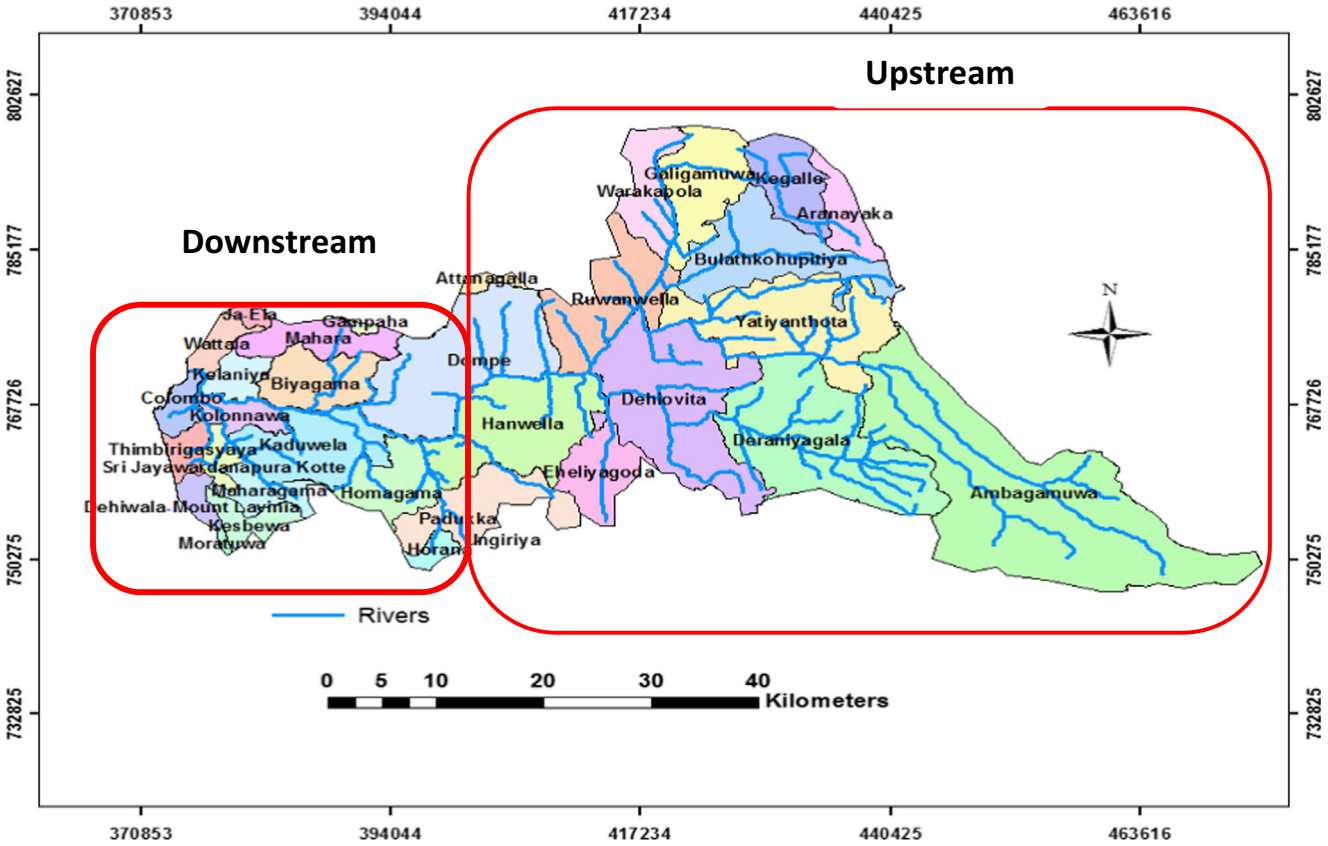

Fig. 1 Study area: Kelani River basin

the four diagonal directions (northeast, northwest, southeast, and southwest). The system computes each velocity of flow independently of the other seven directions, in one dimension, with the stability controlled by the magnitude of the variable computational timesteps (Ahmed and Gerlach 2012; Flo-2D 2009). It calculates the net change in volume as the product of the net change in discharge and timestep; the change in depth is determined by the net change in volume with the surface area of the cell (Ahmed and Gerlach 2012). The model consists of fifteen components: reduction factors, streets, infiltration, inflow and outflow elements, rain, floodplain cross-sections, levees, hydraulic structures, multiple channels, breach, mudflo-2D, mudflow and sediment transport, and evaporation.

Grid development and model inputs

Approximately 2,292km^2 of the basin was divided into two: upper and lower. The upper acts as the inflow source to the lower basin, which causes frequent heavy flooding in the mostly urban and commercially situated areas. The grid was created using elevation data. The topography data were obtained from the Department of Survey, Colombo, from which the digital elevation model (DEM) was developed. The grid cell size of 250 m was assigned to enable fast simulation of the flood events. The roughness coefficients were assigned based on the Chow (1959) rain-runoff model (Table 1) using the landuse map of the study area. Manning coefficients were assigned to the shape file in ArcGIS and exported to the Flo-2D grid where they were computed and distributed within the grid. The Green Amp method of infiltration was used for the simulation. The Green Amp method utilizes initial loss, initial saturation, capillary suction head, hydraulic conductivity, and soil porosity. These components were assigned based on the soil types of the study areas. For the lower Kelani basin, the majority of the soil types (about 70%) are loam. Based on existing literature (De Silva et al. 2012), the capillary suction head, hydraulic conductivity, and soil porosity of loam is 90 mm, 13.2 mm/s, and 0.463, respectively. These were assigned and distributed within the grid.

Hydrology

The discharge, which was used as inflow to the lower Kelani, was derived from the upper Kelani basin. This was simulated using similar hydrologic element response (SHER) model. The modeling system is made up of the submodels of surface, subsurface, and aquifer. The surface model uses kinematic wave equation for surface flow computations, while the subsurface model uses the one-dimensional Richard's equation. For the aquifer model, Darcy's flow is assumed (Herath et al. 1992; Herath et al. 1990; Herath et al. 1995). The modeling

Table 1 Manning's n values assigned to rain-off model (after Chow [1959])

Land cover	Manning coefficient
Urban	0.0.15
Forest	0.035
Crops	0.035
River	0.010
Road	0.016
Crop/grass	0.035

system can be divided into two types of blocks that represent similar hydrologic characteristics, such as recharging and discharging areas. Other sub-block areas, such as impervious, paddy, compressed soil, and compressed soil, can be assigned (Herath et al. 1992). In this study, watershed was divided into two: impervious and pervious blocks. The impervious comprises the roofs, roads paved, and all impermeable materials; the pervious blocks are the paddy fields, croplands, forest, etc.

Governing equations

i.) Impervious Model: this model uses the following equation:

$$\frac{dS_{imp}}{dt} = P - D_{imp} - E_{imp} \tag{3}$$

where P is the rainfall, S_{imp} is the water depth in the depression storage pond, D_{imp} is the surface runoff from the impervious model, and E_{imp} is the evaporation from the depression storage pond. This model makes use of the spill-over from the depression storage pond, as the surface runoff, while the evaporation value is considered small and assumed zero.

ii.) Pervious Model: this model uses three (3) water storage depths, which are computed by the following equations:

$$\frac{dS_1}{dt} = U_s - E_1 - D_s \tag{4}$$

$$\frac{dS_2}{dt} = P - E_2 - R - I - U_s + P_{al} \tag{5}$$

$$\frac{dS_g}{dt} = R - D_g - P_{a2} \tag{6}$$

where S_1 is water storage in the depression pond, S_2 is water storage in the subsurface layer, S_{g} is the water storage in the aquifer, D_{s} is the surface runoff, and E_1 and E_2 are the evaporation from the depression pond and subsurface layer, respectively; P is the infiltration to the subsurface layer (rainfall origin), R is the recharge to the aquifer, I is the interflows, U_{s} is the return flow, D_{g} is groundwater discharge to rivers, P_{a1} is the infiltration to the subsurface layer (irrigation water), and P_{a2} is the water pumped out from a well (Herath et al. 1995).

Data used for the simulation of the hydrology of the runoff at the Hanwella gauge station are the following: (i) rainfall data, (ii) soil parameters (such as saturated hydraulic conductivity [vertical], K0_v, saturated hydraulic conductivity [slope], saturated moisture content, Theta_O, saturated moisture content, Theta_R, Alpha, and Beta),(iii) manning coefficients, and (iv) aquifer parameters. The Kelani River basin was divided in the recharge and discharging blocks as shown in Fig. 2. After the hydrological simulation, the discharges at Hanwella, which is at the start of the flow to the lower basin, were extracted for the flood events (in 2010) and validated with the observed discharges for the same period. Model calibration was done by manipulating the simulation parameters to fit the observed data.

Apart from the failing limb, the peak and the rising limb of the simulated in-flow hydrograph (at Hanwella station) agree well with the observed discharge for the simulated flood event (Fig. 3). The efficiency of the model was assessed using Nash-Sutcliffe model efficiency coefficient (Nash and Sutcliffe 1970), which is defined as:

$$E = 1 - \frac{\sum_{t=1}^{T}\left(Q_o^t - Q_m^t\right)^2}{\sum_{t=1}^{T}\left(Q_o^t - \bar{Q_o}\right)^2} \tag{7}$$

where $\bar{Q}_{\text{o}}$ is the mean observed discharges, Q_{m} is the modeled discharge, and Q_{o}^{t} is the observed discharge at time t. The accuracy of any simulated model, using the Nash-Sutcliffe model, is determined by its closeness to the model efficiency of 1. The efficiency of the simulated model was calculated to be 0.98. This is deemed accurate as it is very close to 1.The output of the calibrated flood hydrograph (Fig. 3) served as the input to flood inundation modeling in Flo-2D, using the control parameters stated in Section 3.1.2.

Channel

Flo-2D's channel flow is simulated in the downstream direction in one dimension. This can be accomplished via trapezoidal, rectangular, or by using surveyed cross-sections, and is routed with the dynamic wave approximation to the momentum equation (Flo-2D 2009).

The channels and their geometry (cross-sections, roughness, channel widths, length of channel, bank

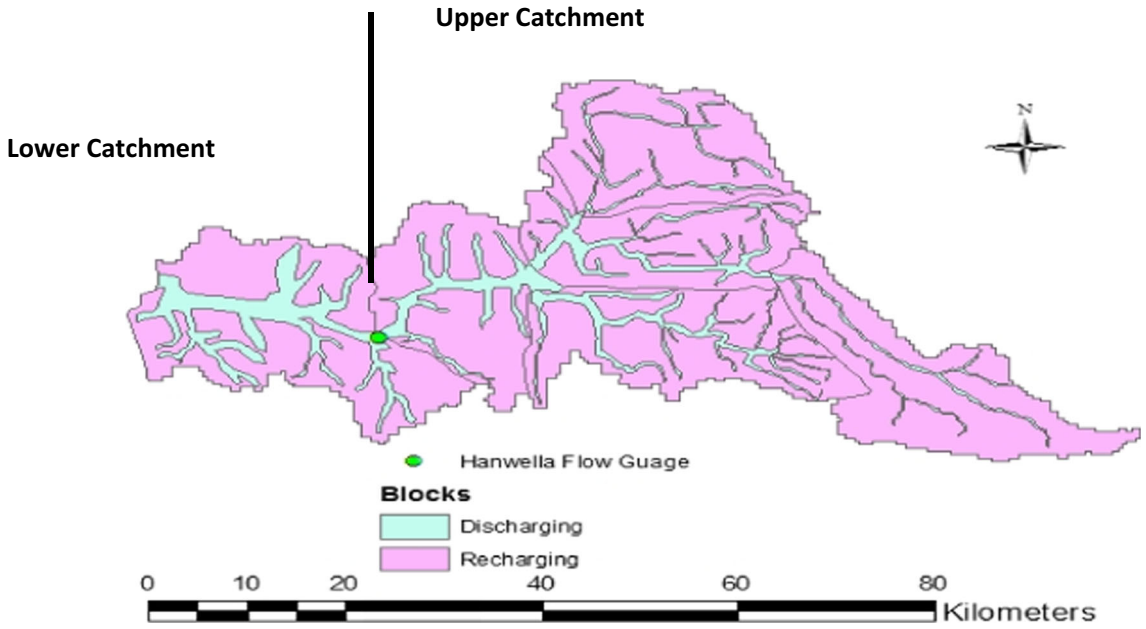

Fig. 2 The recharge and discharge blocks within the upper and lower catchments of the study area

elevations) are represented in the CHAN.DAT file. Only the Kelani Main River, from Hanwella to Nagalagam Street, was considered in the simulation. Channel was delineated in the Flo-2D grid, considering the flow direction from upstream to downstream, and river channel geometry was assigned based on the existing river cross-sections. River cross-sections from Hanwella, Atigala, Kaduwela, Ambatale, Kelanimulla, Wennawatta, and Nagalagam Street were incorporated to simulate the river flow with the floodplain grid elements flow. Hydrograph generated from the upstream at Hanwella served as channel inflow.

Flood simulation

Flood simulation was done in the floodplain mode using various control parameters. In order to ensure numerical stability (a very significant element in flood modeling), stability criteria and floodplain depth tolerance were selected. This was done in the Flo-2D simulation control interface. The default values for the floodplain and channel depth tolerance (DEPTOL), surface detention tolerance (TOL), and the maximum value for the numerical stability coefficient, for dynamic wave routing (WAVEMAX), are 0.2, 0.1, and 1.0, respectively. The model was initially simulated with the default stability parameters by a change to the surface detention tolerance (as 0.015) to improve the stability of the model. Simulation time set for the model was 264 h, accounting for the flood-event period being modeled (May 2010) while the out timestep is 1 h. The simulated inundation model was processed in the Flo-2D Mapper. With this interface, maximum flow depths and the floodplain final

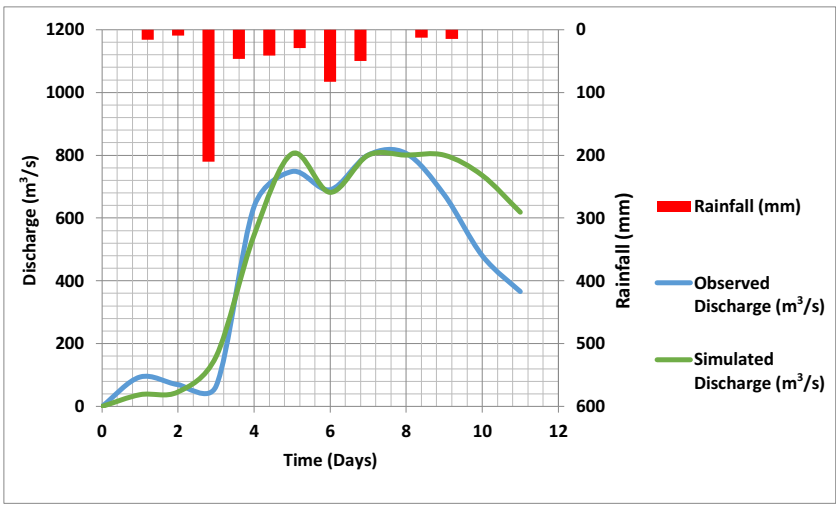

Fig. 3 Simulated vs. observed discharge and the rainfall for the May 14 to May 25, 2010, flood events at Hanwella station

Table 2 Global building types

No.	Category	Descriptions	Identified buildings in the basin
1	Wood	Wood	√
2	All steel structures	Steel light frame	–
3	All concrete frames	Concrete frame with unreinforced masonry infill walls	√
4		Reinforced concrete moment frame	–
5		Reinforced concrete frames and concrete shear	–
6	All masonry	Unreinforced masonry bearing walls	√
7		Reinforced masonry bearing walls	–
8	Adobe	Adobe	–
9	Slab	Flat slab structure	–

flow, as a function of depths, were created from the difference between maximum surface water elevation and the ground surface elevation of the study area. The outputs coded in shape files were exported into ArcGIS for further processing and analysis.

Development of loss functions curves

Building classification

In this study, the initial classification of exposure was based on the global building structural types classifications by the World Agency of Planetary Monitoring and Earthquake Risk Reduction (WAPMERR) as documented by the United Nations office of Disaster Risk Reduction (UNISDR), during a workshop on global risk assessment (Global Assessment of Risk) (Masqsood et al. 2013). (Table 2). UNISDR developed biennial global assessment reports on Disaster Risk Reduction (DRR). These reports contain comprehensive review and analysis of natural hazards and their overall effect on humanity.

At a 2013 GAR workshop, initial benchmark curves for the residential building categories were developed based on expert judgments, which was due to limited existing empirical vulnerability data in different countries.

Field survey and data processing

The survey questionnaire approach was applied in this study to obtain flood damage data for the establishment of loss functions for global residential building types. The field survey was carried out within the flood-prone area in the study basin, aided by the simulated flood map of the area (Fig. 4). A total of 297 flood damage data were collected in the study area on the economic loss impacts on the most recent floods. Respondents are mainly the adult family members with clear remembrance of the recent flood events in the study area. The data include the following: different building classes, repair, and replacement costs of the building structures, with their corresponding flood water heights, water duration, and building floor areas. Other parameters recorded in the field, such as content damages and non-economic impacts, are not included in this study. These data were collected with their corresponding global buildings types identified in the field. The acquired data were processed and analyzed statistically to derive loss functions, which establishes the relationship between structural damage extent and water depths.

Three (3) types of global residential building structures and commercial buildings identified in the field (and corresponding percentage distributions): (i) unreinforced masonry bearing walls (43%), (ii) concrete frame with unreinforced masonry infill walls (41%), (iii) wooden (9%), and (iv) commercial (7%) (see Table 2 and Fig. 5). These structures were recorded with their corresponding flood water depths and damage variables. Damage to structures was calculated based on damage ratio, which is the ratio of the repair cost of the structure after the flood event to the replacement (actual) cost of the structure, as expressed in Eq. 8.

$$Structural\ \ Damage\ \ ratio\ \ (\%) = \frac{Repair\ \ Cost}{Replacement\ \ Cost}^{*} 100 \tag{8}$$

For each category, data were plotted and correlated to derive the best prediction using structural damage as the dependent variable and water depth as the independent variable (the predictor). The models were predicted with logarithm functions expressed in Eq. 9.

$$\mathrm{D}_f = C1 \times ln\,(x) + C \tag{9}$$

where D_f is the damage function, x is the flood water depth (m), and C and C1 are the damage coefficients at any given landuse type (Fig. 12 and Table 6).

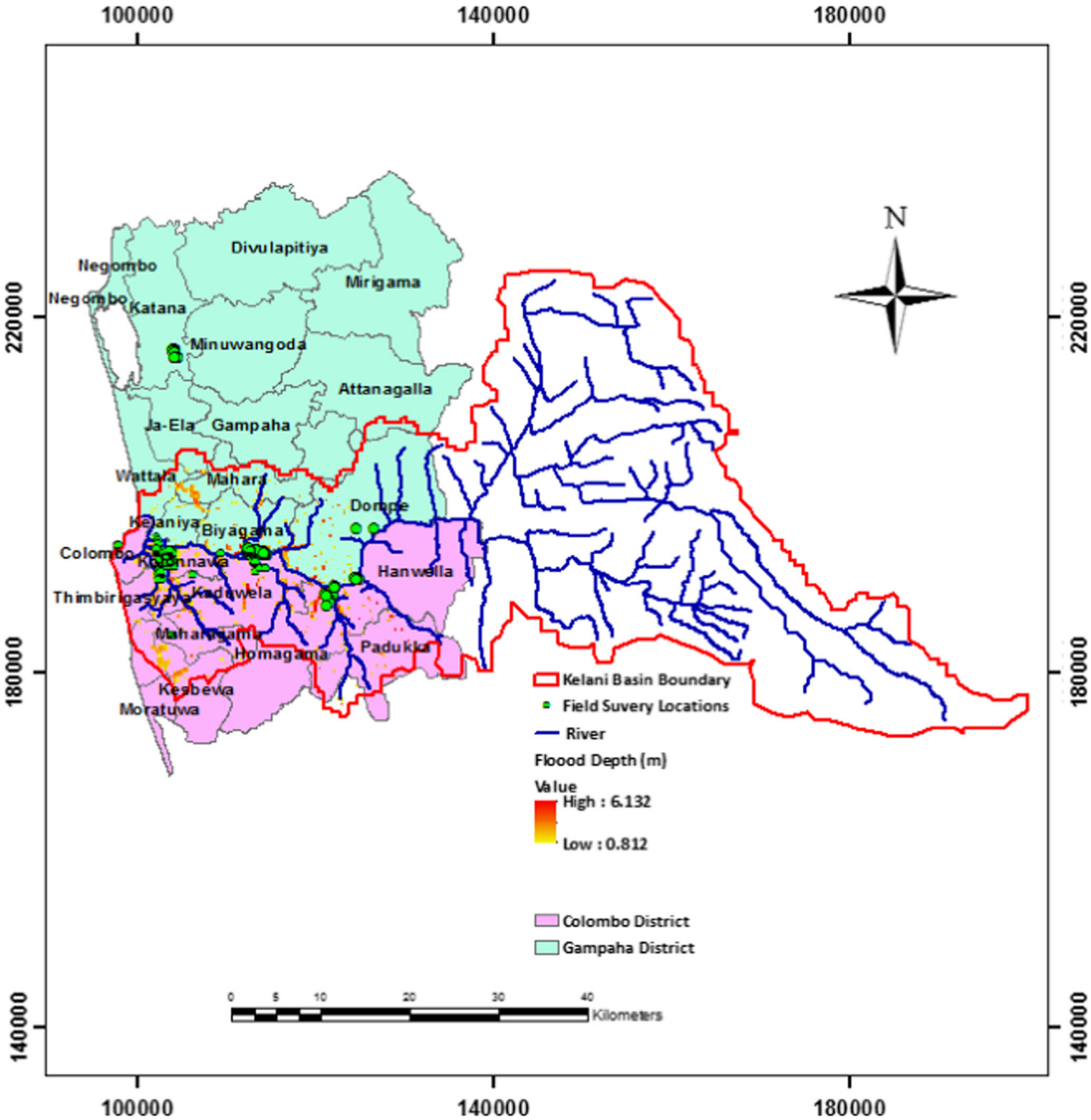

Fig. 4 Field survey locations

Exposures mapping

Built-up extraction from remote sensing data

Building inventory analysis is fundamental in flood disaster risk reduction, planning, and modeling. Flood-risk models require knowledge of the number of buildings within the squared grid for adequate damage or loss estimation (Dutta and Kamrujjaman Serker 2005). In order to carry out the grid-based damage simulation, the distribution of the properties exposed to the flood water depths would be essential. Remote sensing has proven to be an invaluable tool for mapping urban built-up areas (Ahmad et al. 2016; Bhatti and Tripathi 2014; Dutta and Kamrujjaman Serker 2005; Xu 2007). It is a unique technology that provides a synoptic view of the urban area, both in space and time, especially in an inaccessible area where ground survey cannot be carried out (Avtar et al. 2013; Maktav et al. 2005; Richards 2013).

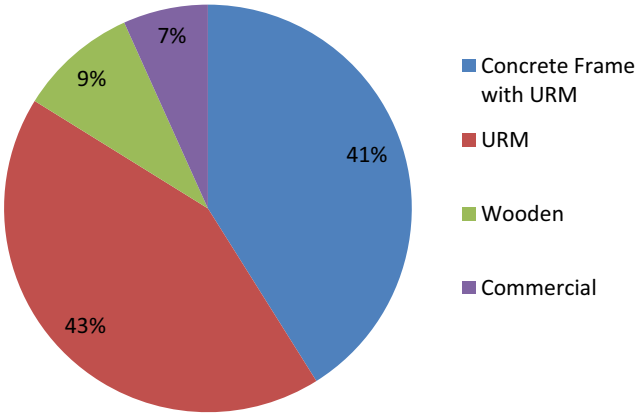

Fig. 5 Surveyed building types and their percentage distributions

Remote sensing data were used to extract the exposure information. Due to limited access to higher resolution data and the cloud cover in the study area, detailed exposure (building) mapping could not be carried out. However, Landsat 8 OLI imagery of the Kelani River basin area (path: 141, row: 55) acquired on April 14, 2015, obtainable from the United States Geological Survey (USGS), was used to extract the built-up areas within the basin. The image (in GeoTiff format), which covers the study area, with less cloud cover (5.07%), consists of eleven (11) spectral bands. Band 1 (coastal aerosol, 0.43–0.45 μm) and band 9 (cirrus, 1.36–1.38 μm) were excluded from further processing because they are not instrumental for the analysis. Landsat 8 OLI optical bands (2–7) are made up of 30-m spatial resolution; thermal bands (10 and 11) was 100 m, but had been resampled to 30 m by the vendors, Earth Resources Observation and Science (EROS) Center, United States Geological Survey (USGS); and band 8 is the panchromatic with a spatial resolution of 15 m. Projection used in this study is Universal Transverse Mercator (UTM) with zone 44 N and WGS datum. The image file extension was image file format (TIFF) and integer, with each band separately downloaded. All the bands (2–8 and 10–11) were layer stacked and clipped to the study area. Areas covered by cloud, within the study area, were considered negligible, and as such no atmospheric corrections were performed. Urban land use is made up of three principal components: the impervious surface materials (built-up), vegetation, and open water. Due to a mixed spectral, as a result of the urban land class heterogeneities, an integrated built-up extraction was applied, using the method developed by Xu (2007). The method incorporated the combination of three (3) thematic-oriented indices that represent three (3) urban land use components: (i) normalized difference built-up index (NDBI), (ii) soil-adjusted vegetation index (SAVI), and (iii) modified normalized difference water index (MNDWI). These components were integrated to effectively differentiate the built-up area from other urban landuse classes in the study area. NDBI was used to generate built area, SAVI was carried out to enhance the vegetation areas, and the MNDWI was analyzed to enhance the water bodies in the study area. All of the thematic images were integrated using principal component analysis (PCA) and threshold technique.

Table 3 Correlation values of the new composite thematic image with NDBI, SAVI, and MNDWI bands

	NDBI	MNDWI	SAVI
NDBI	1	− 0.31156	− 0.82965
MNDWI	− 0.311555	1	− 0.25298
SAVI	− 0.829645	− 0.25298	1

Built-up land extraction

Extraction of built-up land was conducted by integrating the three extracted indices. After the generation of these images (NDBI, SAVI, and MNDWI), a new image was formed by layer stacking the three indices into a single image. The new image reflects the three land cover features in three RGB colors (red: NDBI, green: SAVI, and blue: MNDWI). Correlations between these thematic bands are largely reduced (with the negative correlation as shown in Table 3), consequently with clear distinction among the three major landuse classes: vegetation, water, and built-up land.

PCA was implemented for the extraction of built-up land use from the new layer-stacked thematic image. PCA is a method of identifying patterns in data by highlighting their similarities and differences. It is a process of transforming a set of correlated variables into new uncorrelated variables. Due to its orthogonal transformation, which results in the uncorrelated new images, it is capable of differentiation among the three major landuse classes from the derived thematic image. It examines the principal components (Eigen vectors) to determine which of the image components will relate directly to the spectral signatures of specific target materials (Xu 2007). PCA was performed using forward principal component (PC) rotation to generate three PC images. The RGB color composite of the three PC images clearly differentiate the three landuse classes (Fig. 6). Table 4 shows the Eigen vectors of the transformed images, which are based on the covariant matrix, and determine which of the landuse classes (bands) has the highest influence in the image. In Table 4, PC1 enhances water (positive values) while suppressing the built-up and vegetation (negative values), which cannot be used for the extraction of built-up landuse. PC3 enhances both built-up and water body while suppressing the vegetation; in this case, built-up and water will be mixed up. Only PC2 yields a unique distinction between built-up land (positive values) and the other two classes (negative values). This was utilized for the extraction of built-up land.

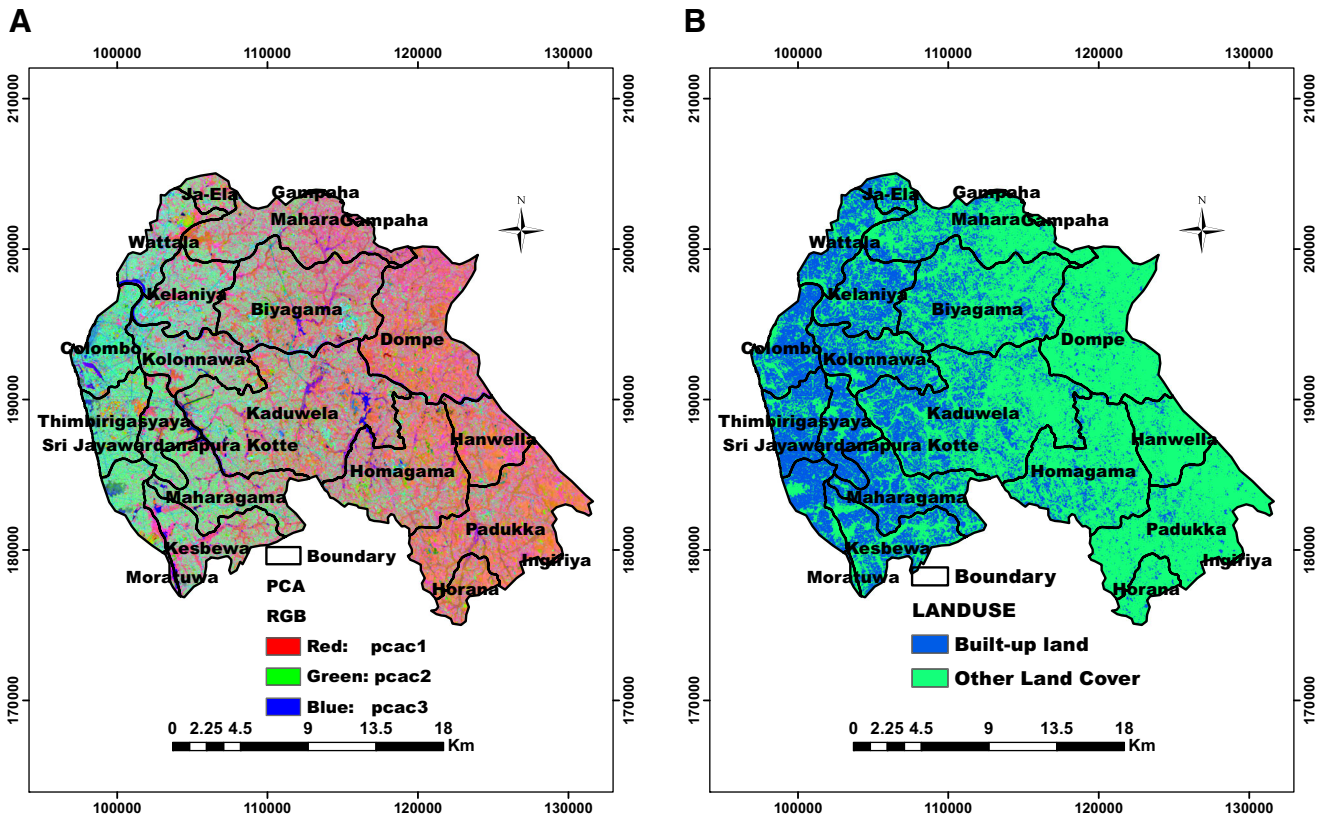

Fig. 6 **a** RGB composite of the PC1, PC2, and PC3. **b** Extracted built-up land

Finally, using threshold value (0.063) based on the Eigen vector of the built-up land, the PC2 image was classified into two: built-up land (values ≥ 0.063) and other land use (< 0.063), as shown in Fig. 6, and these were assigned 1 and 0, respectively. Accuracy of the derived built-up map was examined using confusion matrix. The image was compared with the ground truth data obtained from high-resolution Google earth image, with about 86% accuracy.

Building density estimation

Building density (BD) is defined as the number of building units in any given occupied area. It provides a quantitative measurement of the number of buildings expected within a unit area. In urban planning and development, BD is used as a tool for effective landuse planning, population distribution, and provision of public infrastructures. Landsat8 remote sensing data, as described above, was used to map urban densities in the study area. The Landsat image was classified into five areas: high dense urban, medium dense urban, low dense urban, water bodies, and vegetation as shown in Fig. 7. The high dense urban is mostly concentrated in Colombo, Sri Jayewardenepura Kotte, and Thimbirigasyaya divisional secretariats. Areas covered by water bodies and vegetation were not included in the density estimation. Only the area of urban classes (high dense, medium dense, and low dense) and the total number of buildings in 18 divisional secretariats (obtained from the Department of Census and Statistics, Sri Lanka) were combined in multiple linear equations (Eq. 10, Table 5) to derive the BD for the three urban classes.

Table 4 Principal components analysis (PCA) of the thematic bands

Eigen vectors	Bands	PC1	PC2	PC3
	NDBI	−0.7439	0.0633	0.6653
	MNDWI	0.2518	−0.8956	0.3667
	SAVI	−0.6191	−0.4403	−0.6503

$$B_i = \beta_i x + \omega_i Z + \delta_i Z, For = 1, 2, 3, 4, 5.....n \quad (10)$$

$B_i$is the total number of buildings (residential and commercial); β_i, ω_i, and δ_i are areas (km^2) covered by high dense urban, medium dense urban, and low dense urban, respectively; $x, y, and\ z$ are the BD (number of buildings per km^2) for high dense urban, medium dense urban, and low dense urban, respectively (Fig. 8)

We estimated the BDs for the high, medium, and low urban to be 4254, 1450, and 1162 buildings per square kilometer, respectively. These were further validated by multiplying each estimated BD by the land cover area for the density classes in each secretariat and compared with the measured number of buildings. Both the observed and estimated total number of

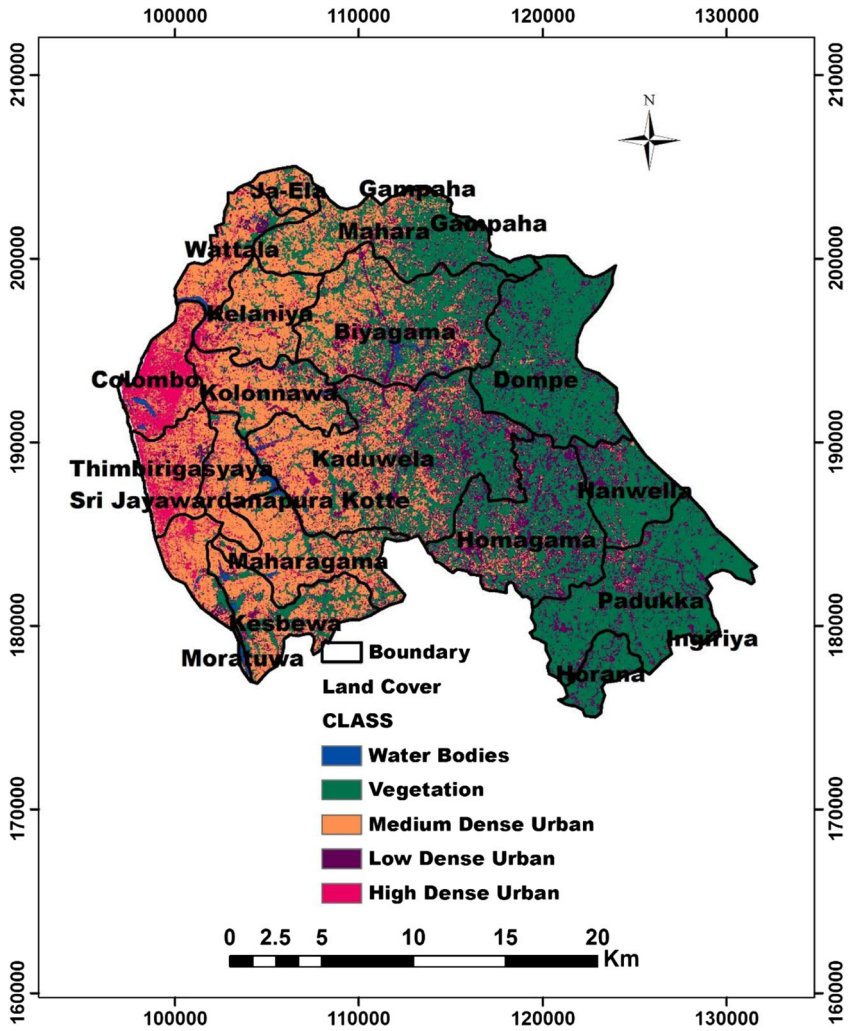

Fig. 7 Landuse classes derived from image classification

buildings showed good agreement (Fig. 9). The BDs were spatially distributed within the grid for flood damage estimation.

GIS-based flood damage modeling

Detailed loss functions established in this study were applied to the Kelani River basin and validated by the observed damage obtained after the flood disasters in May 2010. Lower Kelani River basin, which is the urban area mostly affected by flood, was considered for the application of the loss models developed in this study. The basin is comprised of two main districts: Colombo and Gampaha. Colombo District, which is host to the commercial capital city, Colombo, is the most densely populated district and also the most urbanized in the river basin. The total population of all the twenty sub-districts within the basin, according the Population Census (2012), is estimated to be 3,291,600. A GIS Grid-Based modeling was employed to simulate the total damages using the established loss functions (Fig. 10). Estimation of damage requires a dynamic link between the flood characteristics (obtainable from the flood inundation model) to the damage estimation model. Apart from flood characteristics, such as flood depths and stage-damage function, a grid-based flood damage model requires various spatial data inputs, such as the exposures distribution, BD, floor area, cost of structure per unit area, and ratio of structural building type in the study area. These spatial data were derived from flood simulation analysis (e.g., flood depths) of remotely sensed data and building information available at the Census and Statistics Department and Disaster Management Centre, Ministry of Disaster Management, Sri Lanka (e.g., urban land cover, building density, unit costs, and floor area). The design of a damage estimation model must be made to directly input the flood inundation model grid outputs (Dutta et al. 2003). Dutta et al. (2003) formulated mathematical models for various urban damage categories (residential and non-residential), which can be used to simulate flood damages in any basin. In this study, their concept for the building structural damage estimation was applied. The model made use of the floor area concept because the economic value of a building structure is defined by the unit floor area and defined as follows:

Table 5 Area covered by urban density types for each secretariat and their total number of buildings

Secretariats	High dense urban (km^2)	Medium dense urban (km^2)	Low dense urban (km^2)	Total number of buildings
Bigiyama	0.88	19.6	13.5	48,090
Thimbirigasyaya	6.93	9.89	1.7	52,763
Sri Jayewardenepura	1.44	12.04	1.4	27,144
Moharagama	0.79	19.38	4.2	49,459
Kolanniwa	1.77	15.88	3.8	44,663
Kelaniya	1.47	16.83	2.6	33,404
Kaduwela	1.35	32.26	22.1	64,791
Colombo	11.8	6.09	1.3	65,831
Homagama	0.50	12.21	34.6	61,505
Dompe	0.29	1.66	25.1	39,369
Padukka	0.17	0.67	13.3	17,007
Hanwella	0.42	1.75	20.8	25,461
Kesbewa	0.71	25.81	11.2	62,653
Dehiwala	3.96	14.55	2.1	22,352
Mahara	0.19	18.93	8.3	52,897
Ja-Ela	0.76	32.44	11.9	52,358
Gampaha	0.21	20.85	13.2	51,111
Watala	3.74	26.30	9.8	43,170

$$D_{s(i,j)} = \sum_{k=1}^{n} \left[N_s(i,j,k)^* FA(i,j,k)^* EC_s(i,j,k)^* C_s(i,j,k) \right] \quad (11)$$

A further modification was done to the damage estimation model using BD and the building ratio concept in order to disaggregate the various global building types within the grid. The above equation is modified as:

$$D_{s(i,j)} = \sum_{k=1}^{n} \left[BD(i,j,k)^* BR(i,j,k)^* FA(i,j,k)^* EC_s(i,j,k)^* C_s(i,j,k) \right] \quad (12)$$

where, for any grid (i, j)

D_s (i, j)	total damage to structure
n	total number of types of building structure
N_s	total number of building units of structure type k
BD (i, j, k)	building density (building units/km^2)
BR (i, j, k)	ratio of building type k
FA	average floor area per building unit of structure type k
EC_s	estimated cost of a building of structure type k per unit area
C_s	Depth-damage function for building structure type k

In Sri Lanka, the replacement cost of residential buildings ranges from 2000 to 4000 LKR/square feet, according to building construction associations. The lower end of the cost is predominantly in the medium and low urban areas, which are most affected by flood. The higher end of the cost is in the high-dense urban area. In order to reflect the construction scenario in the basin, we simulated flood damages based on the price of $165 per square meter. We used the average floor area from the urban and semi-urban area, as reported by the Department of Census and Statistics, and also from the field work carried out in the study area. The 2010 census reported that a 64.5% proportion

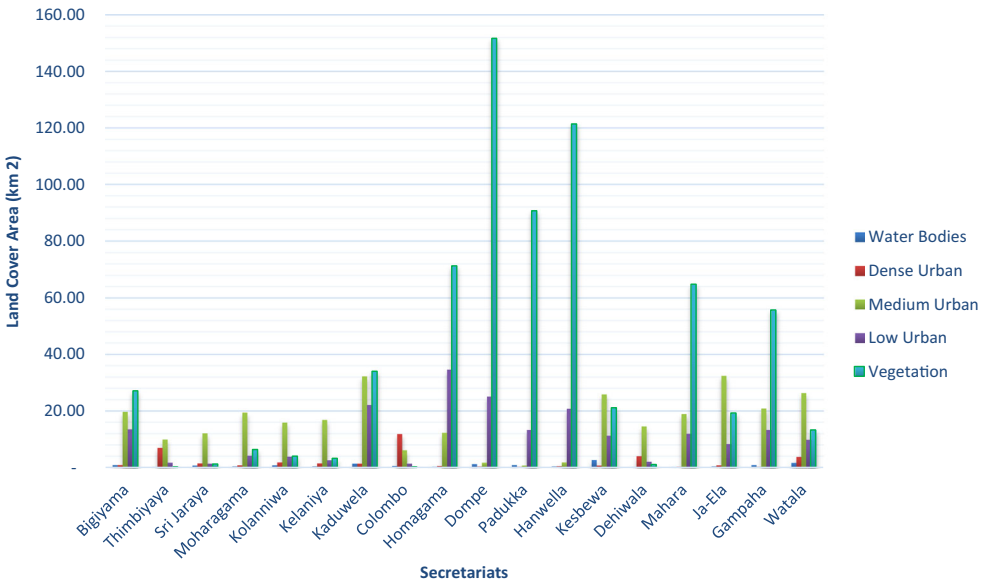

Fig. 8 Graphical representation of five (5) land cover classes in the study area

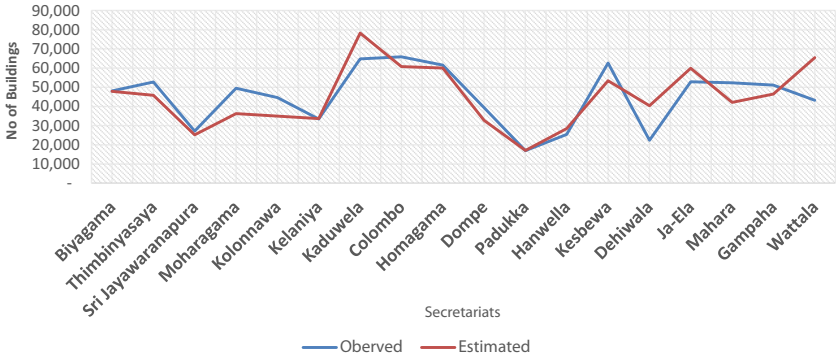

Fig. 9 Estimated number of buildings vs. observed number of buildings

of household units that are within the floor area are greater than or equal to 500 square feet (46 square meter) in Sri Lanka (Census and Statistics Department 2012); whereas about 36.5% occupied less than 500 square feet (46 square meter). The census report shows no much difference between the urban and rural area in terms of floor area occupied by the residential buildings. Quite a large proportion lives between 500 and 750 square feet. Based on the statistics and the field work data, the average floor area of 600 square feet (56 sq m) for both urban and semi-urban areas was used.

Results and discussion

Flood hazards

Figure 11a shows the simulated flood inundation for the flood event (May 2010) in the basin. The extracted maximum flood depths range from 0.8 to 6.2 m. The highest flood heights are experienced along the river's course, mostly in Hanwella, Dompe, and Biyagama. The lowest water heights are experienced in the Colombo area. Simulated inundation extents were compared with observed data from the May 2010 event (Fig. 11b). The observed flood inundation was obtained from ALOS PALSAR 1.5 data product, by Japanese Aerospace Exploration Agency (JAXA) at 6.3-m ground resolution, on May 18, 2010. The extracted observed flood inundation area from PALSAR data as at 18th May 2010 is 53.9km^2; whereas the simulated total inundated area is about 65.4km^2, which extends to all of the administrative boundaries within the basin. Both of the simulated inundation extents match well with the observed inundation. The simulated flood water along the rivers especially in the upstream, agree fully with the observed data. In the downstream part of the inundation map, around the Kolonnawa and Colombo areas, more flood water can be seen in the left bank of the Kelani River compared with very little flood water in the observed data. One of the reasons for this could be the topography data used, which may produce different estimated slopes from what is obtainable on the ground. Another reason could be the resolution used in the simulation, which is 250 m, a rather coarser resolution compared to the observed flood data at 6.3 m. The effect of resolution on the spread and the depths of flood water have been investigated in recent studies (Dutta and Nakayama 2009; Podhorányi et al. 2013). Generally, simulating at coarse resolution would affect the extent/spread of the water and the

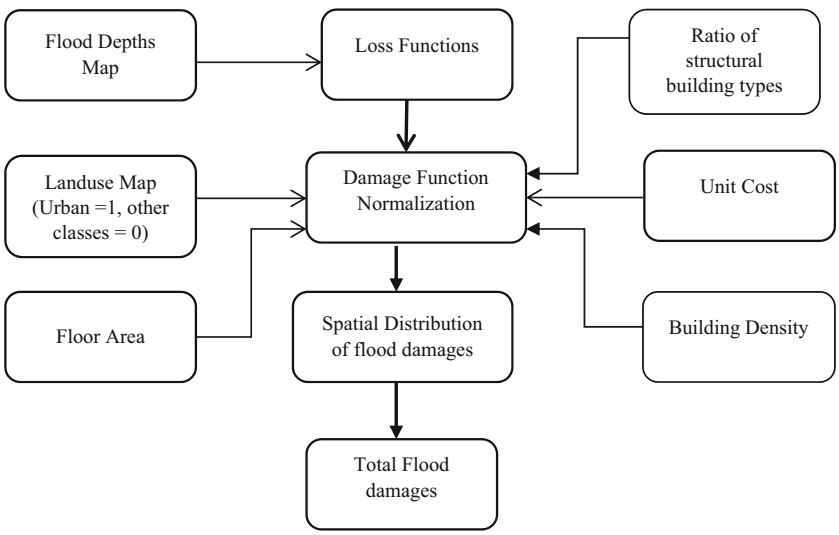

Fig. 10 GIS-based flood damage simulation flow

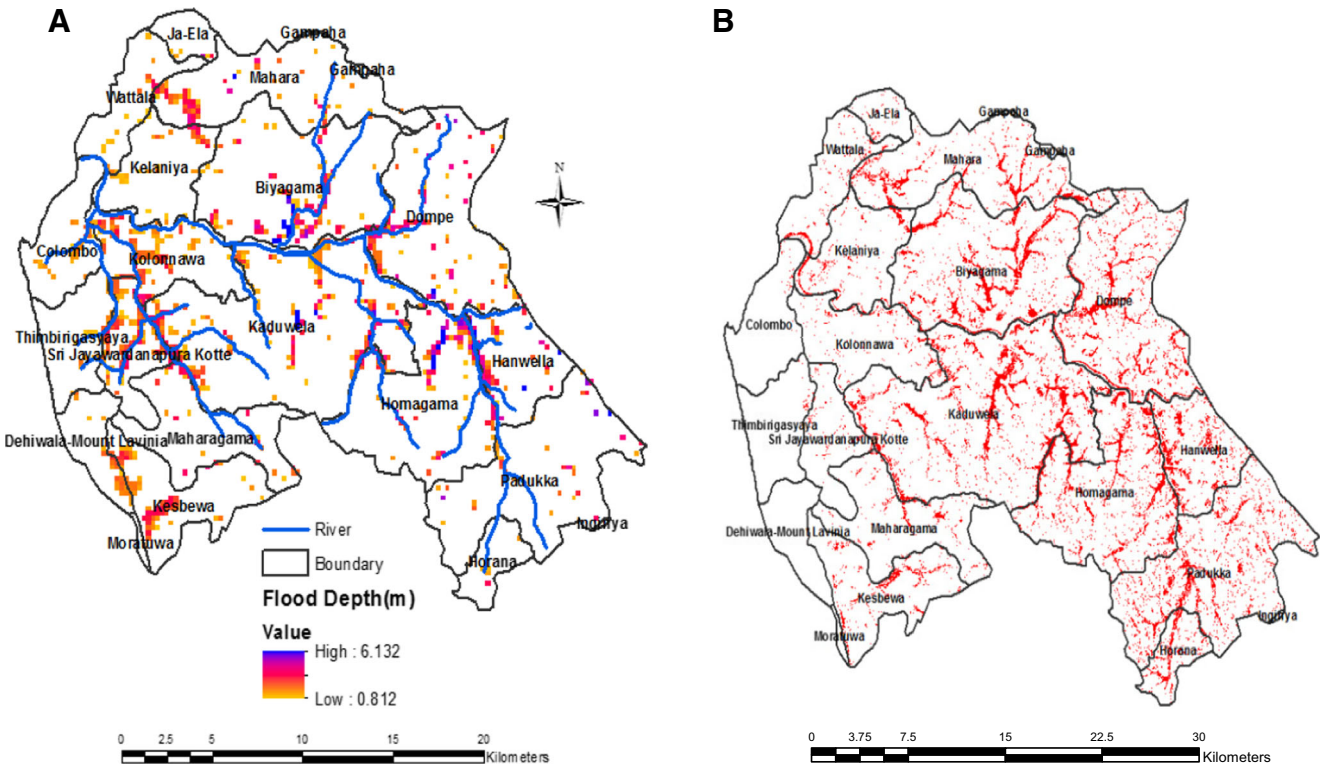

Fig. 11 **a** Simulated flood inundation depths. **b** Observed flood inundation

water heads. The simulation in this study was done at 250-m grid resolution because of available computer resources and the required time to accomplish the simulation over a large basin like the study area. High resolution with accurate topography data would produce higher accuracy in flood simulation.

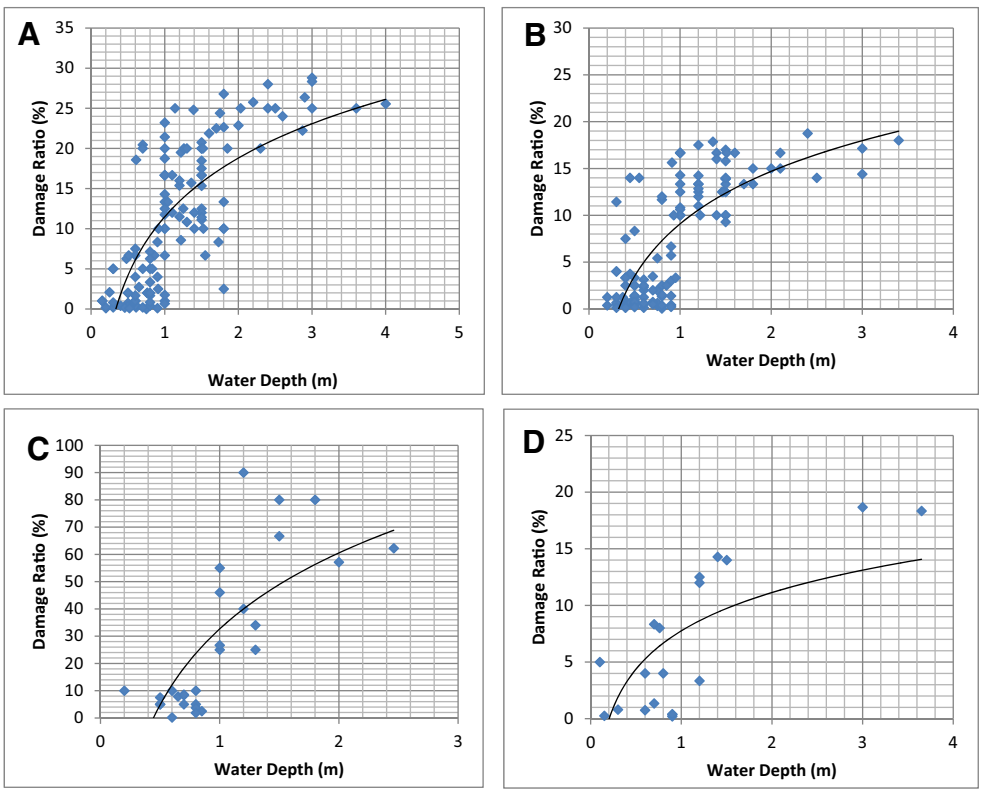

Fig. 12 Flood damage curves for the following. **a** Residential unreinforced masonry (URM). **b** Residential concrete frame with unreinforced masonry walls. **c** Residential wooden structure. **d** Commercial building

Table 6 Derived flood damage coefficients

Building types	C1	C
Unreinforced masonry walls (URM)	10.55	11.487
Concrete frame with unreinforced masonry fill walls	8.0826	9.0925
Wooden	40.211	32.656
Commercial building	4.8745	7.7563

Vulnerability functions

Figure 12 shows the degree of flood damage expected at a given flood depth for each of the global building structural types. The damage ratio for the building categories slightly varies. The wooden and unreinforced masonry walls show maximum damage ratio as explained by the applied model at 70 and 26%, respectively, while the concrete frame with unreinforced masonry walls revealed maximum damage at 19%. The commercial structures are predicted at 14%. The degree of damages in each of the building categories shows the responses of different building materials to water depths. From the model, wooden and unreinforced masonry walls are more vulnerable to flood than the concrete frame with unreinforced masonry. Wooden structures are typically highly vulnerable to water and are expected to have higher damage ratio with respect to flood water height. The flood damage coefficients (C1 and C) for all the building as defined by the logarithm model in Eq. 9 as listed in Table 6.

Flood damage estimates and model validation

Simulated damages are $64,065, $248,096, and $331,012 for residential wooden, concrete frame with unreinforced masonry (CFURM), and unreinforced masonry walls (URM) structures, respectively (Fig. 13). The wooden (despite the highest vulnerability to flood) accounts for the lowest damages in the basin. This is because of the scanty distribution of wooden structures in the study area. Expectedly, URM (the predominant structures with relatively high vulnerability) showed the highest damages, followed by the CFURM. Damages to commercial buildings, mostly made up of concrete structures, are estimated to be $42,358.

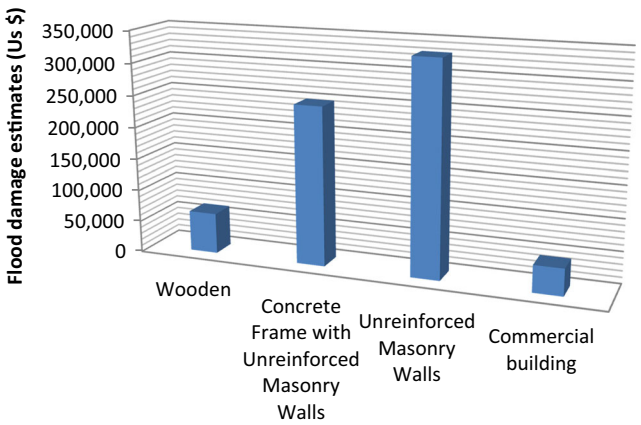

Fig. 13 Estimated total flood damages for different building types

Models validation

In 2010, between May 12 and May 21, heavy rainfall resulted in a devastating flood that affected about five districts (Colombo, Gampaha, Kalutara, Galle, and Matara) out of Sri Lanka's 25 districts (DMC 2010). According to DMC (2010), the value of damages and losses was estimated at LKR 5,059 million or $46 million. Kelani River basin, which is comprised of mainly Colombo and Gampaha districts, accounts for a total of LKR 90 million ($750,188) worth of damages to house structures, LKR 28 million worth of damages to household goods, LKR 26 million for the cost of shelter, and LKR 116 million for clean-up costs (Table 7).

Table 8 shows the simulated damages for all of the three (3) global building structural types in the study area, in comparison with the post-flood survey damages estimated by the Disaster Management Centre, Ministry of Disaster Management, Sri Lanka (DMC). Damages to commercial structure cannot be verified in this study because of lack of detailed observed damage for commercial building. It can be observed from the aggregated simulated damages to residential structures that they are lower than the damages from the post-flood field survey by about 17% (Fig. 14). This difference can be attributed to the fact that the extent of damages in the lower Kelani basin, though comprised of two major Districts (Colombo and Gampaha), does not fully encompass all of the secretariats in the districts, especially Gampaha in the northern part, which recorded higher damages according to the observed damage reports (see Fig. 4). Assuming that all of the secretariats are within the lower basin, it is expected that the simulated damages will be a slightly higher (about 30%) than the observed damages. This expected higher damage can be attributed to the difference in the extent of the simulated inundation and the observed map.

Since the simulated lower Kelani basin covers most parts of Colombo district (see Fig. 4), it will be much better to compare the observed and estimated damages for Colombo district. Figure 15 shows the comparison between the observed and the estimated damages for Colombo district. It can be observed that the estimated damages exceed the observed damages with about 30%. The reason, as earlier mentioned, could be the grid resolution (250 m) used in the simulation. Also, some other factors, such as the detention basin, buildings, and some locally elevated highways, which were not considered in the simulation, can be a major cause of the large difference. Estimation of property exposure is an important factor that can be attributed to the difference. The study made use of Landsat-8 OLI with 30-m resolution to extract the build-up areas in the basin and the estimation of urban density.

Table 7 Observed damages (May 2010 flood event) to housing by district (LKR million) adapted from DMC (2010)

	Damages to houses structures	Damages to household goods	Shelter costs	Clean-up costs
Colombo	44	13	11	54
Gampaha	46	15	15	62
Total	90	28	26	116

Higher resolution imagery, as suggested by Komolafe et al. (2015), would be necessary, especially when the flood heights are simulated at coarse resolution. Despite the uncertainty sources, the performances of the loss models are near accurate and can be used for future approximate estimation of flood damages for risk planning and prevention.

From the results, it clearly shows that the empirically generated loss functions through field survey can provide more accurate flood damage forecast if past observed/surveyed flood damage data are available for model calibration and validation. The loss functions were able to predict of about 70% of the observed total flood damages of May 2010 flood event in the Kelani River basin. Meaning that, by using the three loss functions and the spatial data components in this study, 70% of the future flood damages can be predicted. However, more accurate results can be achieved if higher resolution remote sensing data is used for the mapping of the urban property distribution and ambiguities in the inundation modeling are reduced.

Conclusions

In this study, four vulnerability (damage) curves for floods were developed for global building types using an empirical approach applied to the Kelani River basin in Sri Lanka. This was done with the aim of differentiating economic losses associated with each element at risk (de Moel et al. 2012) and

Table 8 Simulated damages based on global building types vs. the observed total damages

Residential building types in the River basin	Simulated flood damages (USD)	Observed flood damages (USD) to residential structures
Wooden	$64,065	
Concrete frame with unreinforced masonry walls	$248,096	
Unreinforced masonry walls	$331,012	
Total damages to residential structures	*$643,173*	*$750,188*
Commercial building structure	$42,358	

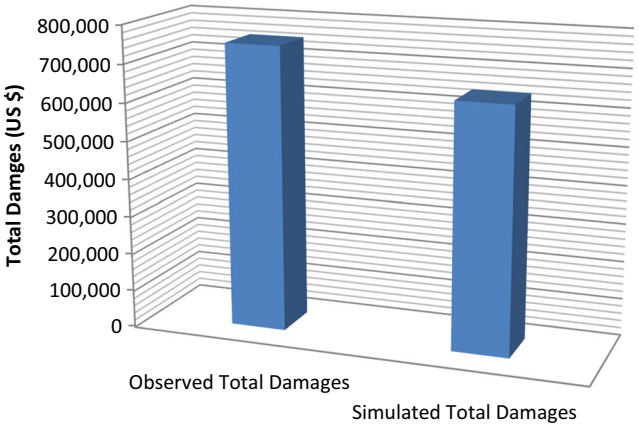

Fig. 14 Simulated vs. observed total damages for residential structures

generating input data to the regional or global risk model for risk comparison and mobilization of international supports for risk reduction and management. The flood inundation was simulated using Flo-2D, a grid-based hydrodynamic flood model, which considered major physical occurrences in the river basin. An event-based (May 2010) flood modeling was applied in order to validate the established loss functions. A modified integrated mathematical model, which provides a dynamic link between the simulated flood and the established detailed loss functions, was used to provide spatial distribution of flood losses for each residential building structure in the study area. This paper has demonstrated the possibility of differentiating economic losses (in each structural damage category), instead of the usual aggregated losses that are more commonly documented. The results of the inundation simulation, to some extent, match with the observed flood map and show the capability of the Flo-2D model in estimating flood inundation parameters over a relatively large basin like the study area.

The slight difference in the flood extent of the simulated and the observed flood map could be as a result of the inability to incorporate other factors, such as buildings, detention basin, street, and groundwater. Due to the size of the river basin and

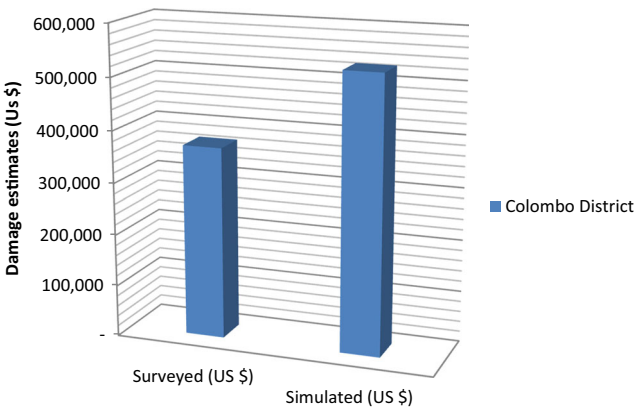

Fig. 15 Simulated vs. observed total damages for residential structures for Colombo District

in order to ensure a faster grid simulation, a grid size of 250 m was used in the simulation. This, in addition to previous factors, could have resulted in some level of ambiguity in the simulated model. Further improvement in the future can consider and/or mitigate these factors for enhanced simulation. The maximum vulnerability index predicted by the model for the building types in the study areas showed 0.7, 0.26, 0.19, and 0.14, for wooden, unreinforced masonry walls (URM), concrete frame with unreinforced masonry walls (CFURM), and commercial structures, respectively. This revealed the damage responses of the building structures to flood water, which is dependent on the materials of the buildings and the water depths. As expected, woods are more susceptible to flood water, and hence has the highest vulnerability index, followed by the URM, CFURM, and commercial structures.

It is intended that the empirically established loss functions can be incorporated at the regional scale for developing regional-specific functions. Apart from providing input data for regional flood-risk modeling, the established model can also be transferable and applicable to other countries for comparing flood risk associated with similar building materials and types. This can be done by normalizing the floor area and country or the regional replacement cost. The generalized loss functions can be employed for estimating future losses to flood and to evaluate the influence of climate change on potential flood damages, as well as for understanding the relative impact on a given country's economy. This is very essential for decision making by governmental agencies and investors for collaborating and planning for disaster risk reduction.

Acknowledgements We appreciate the Japan Foundation for UNU and the CECAR ASIA for providing funds for this research. FLO-2D Software, INC is appreciated for supporting this research and Flo-2D software, respectively. Much thanks to the Japan Aerospace Exploration (JAXA) for providing satellite data for this study.

References

Ahmad S, Avtar R, Sethi M, Surjan A (2016) Delhi's land cover change in post transit era. Cities 50:111–118

Ahmed I, Gerlach RM Distributed flow guided dydraulic modeling of a desert river system for flood control, *in* Proceedings River Flow 2012, Costa Rica San Jose, 2012, 1, Taylor and Francis Group, LLc, p. 1007–1015

Avtar R, Takeuchi W, Sawada H (2013) Full polarimetric PALSAR-based land cover monitoring in Cambodia for implementation of REDD policies. Int J Digital Earth 6(3):255–275

Bhatti SS, Tripathi NK (2014) Built-up area extraction using Landsat 8 OLI imagery. GI Sci Remote Sens 51(4):445–467

Cammerer H, Thieken A (2013) Historical development and future outlook of the flood damage potential of residential areas in the Alpine Lech Valley (Austria) between 1971 and 2030. Reg Environ Chang 13(5):999–1012

Cammerer H, Thieken AH, Lammel J (2013) Adaptability and transferability of flood loss functions in residential areas. Nat Hazards Earth Syst Sci 13(11):3063–3081

Census (2012) Census of Pupolation and Housing: Department of Census and Statistics, Ministry of Finance and Planning

Chow VT (1959) Open-channel hydraulics. Blackburn Press, Calwell

de Moel H, Asselman NEM, Aerts JCJH (2012) Uncertainty and sensitivity analysis of coastal flood damage estimates in the west of the Netherlands. Nat Hazards Earth Syst Sci 12(4):1045–1058

De Silva MMGT, Weerakoom SB, Herath S, Ratnayake UR (2012) Event Based Flood Modeling in Lower Kelani Basin, in Proceedings SAITM Research Symposium on Engineering Advancements, Malabe, Sri Lanka

DMC (2010) Integrated Post Flood Assessment: Disaster Management Centre, Ministry of Disaster Management

Dutta D, Herath S (2001) GIS Based Flood Loss Estimation Modeling in Japan, in Proceedings Proceedings of the US-Japan 1st Workshop on Comparative Study on Urban Disaster Management, Port Island, Kobe, Japan, February 2001

Dutta D, Herath S, Musiake K (2003) A mathematical model for flood loss estimation. J Hydrol 277(1–2):24–49

Dutta D, Kamrujjaman Serker NHM (2005) Urban building inventory development using very high resolution remote sensing data for urban risk analysis. Int J Geoinform 1(1):109–116

Dutta D, Nakayama K (2009) Effects of spatial grid resolution on river flow and surface inundation simulation by physically based distributed modelling approach. Hydrol Process 23(4):534–545

Flo-2D (2009) Flo-2D Reference manual, *in* FLO-2D Software, I., ed.: Nutrioso

Freni G, La Loggia G, Notaro V (2010) Uncertainty in urban flood damage assessment due to urban drainage modelling and depth-damage curve estimation. Water Sci Technol—WST 61(12):2979–2993

Giang NT, Chen J, Phuong TA (2009) A method to construct flood damage map with an application to Houng River basin, Central Vietnam. VNU J Sci, Earth Sci 25:10–19

Heisten M, Davdge D (2005) Flood damage estimation in the Upper Themes River Watershed. University of Western Ontario and University of Waterloo, Waterloo

Herath S, Dutta D, Musiake K (1999) Flood damage estimation of an urban catchment using remote sensing and GIS, *in* Proceedings International Conference on Urban Storm Drainage, Volume 4, p. 2177–2185

Herath S, Hirose N, Matsuda S (1992) A process model for basin hydrological modelling and its application, *in* Proceedings Japan Annual Conference of Society of Water Resources and Hydrology,, p. 146–149

Herath S, Hirose N, Musiake K (1990) A computer package for the estimation infiltration capacities of shallow infiltration facilities, *in* Proceedings 5tt International Conference on Urban Storm Drainage, Japan, p. 111–118

Herath S, Ni G, Babar B, and Musiake K (1995), Investigation of scaling effect in hydrologic modeling using distributed hydrologic models, *in* Proceedings 2nd Study Conference on GEWEX Asian Monsoon Experiment, Thailland, 6–10, March 1995, p. 207–211

Herath, S., and Wang, Y., 2009, Incorporating wind damage in potential flood loss estimation: Global Environmental Research p. 151–159

Islam MM, Ado KS (2000) Flood damage and management modelling using satellite remote sensing data with GIS: case study of Bangladesh, *in* Proceedings Remote Sensing and Hydrology 2000 (Proceedings of a symposium held at April 2000). IAHS Publ. no. 267, 2001, Santa Fe, New Mexico, USA,

James L, Hall B (1986) Risk information for floodplain management. J Water Resour Plann Manag 112(4):485–499

Jongman B, Kreibich H, Apel H, Barredo JI, Bates PD, Feyen L, Gericke A, Neal J, Aerts JCJH Ward PJ, (2012) Comparative flood damage

model assessment: towards a European approach: Nat. Hazards Earth Syst. Sci.,, v. 12, p. Nat. Hazards Earth Syst. Sci.,

Jonkman SN, Bočkarjova M, Kok M, Bernardini P (2008) Integrated hydrodynamic and economic modelling of flood damage in the. Netherlands: Ecological Economics 66(1):77–90

Kelman, I., and Spence, R., 2004, An overview of flood actions on buildings: Eng Geol, v. 73, no. 3–4, p. 297–309

Kimura K, Ishimi K, Sato S, Fukuda T, Mikami T, Kikuchi S (2006) Verification of tsunami wave source model and formulation of vulnerability function for buildings based on the investigation of actual damage due to the Sumatran earthquake and tsunami: subject area bein the damage at Matara city. Sri Lanka: Costal Eng Committee 53:301–305

Komolafe AA, Srikantha H, Avtar R, (2015) Sensitivity of flood damage estimation to spatial resolution: journal of flood risk management, p. https://doi.org/10.1111/jfr1113.12224

Kreibich H, Thieken AH, Petrow T, Muller M, Merz B (2005) Flood loss reduction of private households due to building precautionary measures—lessons learned from the Elbe flood in August 2002. Natural Hazards Earth Syst Sci 5(1):117–126

Maktav D, Erbek FS, Jurgens C (2005) Remote sensing of urban areas. Int J Remote Sens 26(4):655–659

Masqsood T, Wehner M, Ryo H, Edwards M, Dale K, Miller V (2013) GAR 15 Regional Vulnerability Functions: Reporting on the UNISDR/GA SE Asian Regional Workhop on Structural Vulnerability Models for GAR Global Risk Assessment, 11–14 November, 2013, : Geoscience Australia

Merz B, Kreibich H, Schwarze R, Thieken AH (2010) Assessment of economic flood damage. Nat Hazards Earth Syst Sci 10:1697–1724

Ministry of Irrigation Resources, S. L., 2009, Proposed Kaluganga Multipulse development Project.: Department of Irrigation, Water Resources abd Planning, Ministry of Irrigation and Water Management

Moel, H., and Aerts, J. C. J. H., 2011, Effect of uncertainty in land use, damage models and inundation depth on flood damage estimates: Nat Hazards, v. 58, no. 1, p. 407–425

Murao O, Nakazato H (2010) Vulnerability functions for Buildings Based on Damage Survey Data in Sri Lanka after the 2004 Indian Ocean Tsunami, in Proceedings International Conference on Sustainable Built Enviroment (ICSBE), Kandy,

Nash JE, Sutcliffe JV (1970) River flow forecasting through conceptual models part I—a discussion of principles. J Hydrol 10(3):282–290

Niroshine MAC (2012) Adaptation to Extreme Floods Under Future Climate Change Scenarios for Colombo, Sri Lanka, International Forum for Sustainable Asia and the Pacific: Yokohama, Japan

Niroshinie MAC, Babel MS, Herath S (2011) A methodology to analyze extreme flooding under future climate change scenarios for Colombo, Society for Social Management Systems Internet Journal, Society for Social Management Systems

Notaro V, De Marchis M, Fontanazza CM, La Loggia G, Puleo V, Freni G (2014) The effect of damage functions on urban flood damage appraisal. Procedia Eng 70(0):1251–1260

Peris N (2006) Vulnerability functions for tsunami loss estimation, *in* Proceedings 1st European Conference on Earthquake Engineering and Seimology, Volume 1121

Podhorányi M, Unucka J, Bobál P, Říhová V (2013) Effects of LIDAR DEM resolution in hydrodynamic modelling: model sensitivity for cross-sections. Int J Digital Earth 6(1):3–27

Richards JA (2013) Remote sensing digital image analysis: an introduction. Springer, New York

Xu H (2007) Extraction of urban built-up land features from Landsat imageries using a thematic-oriented index combination technique. Photogramm Eng Remote Sens 73(12):1381–1390